Applied Catalysis B: Environmental 147 (2014) 402–410

Contents lists available at ScienceDirect

Applied Catalysis B: Environmental

journal homepage: www.elsevier.com/locate/apcatb

Effect of calcination/reduction conditions of Ni/La_2O_3–αAl_2O_3 catalyst on its activity and stability for hydrogen production by steam reforming of raw bio-oil/ethanol

Beatriz Valle*, Borja Aramburu, Aingeru Remiro, Javier Bilbao, Ana G. Gayubo

Chemical Engineering Department, University of the Basque Country, P.O. Box 644, 48080 Bilbao, Spain

ARTICLE INFO

Article history:
Received 9 July 2013
Received in revised form
13 September 2013
Accepted 16 September 2013
Available online 25 September 2013

Keywords:
Bio-oil reforming
Ethanol
Hydrogen
Ni/La_2O_3–αAl_2O_3
Catalyst preparation

ABSTRACT

The influence of calcination and reduction temperatures of Ni/La_2O_3–αAl_2O_3 catalyst used in the steam reforming of raw bio-oil was studied in the 550–850 °C range. The experiments were conducted by continuously feeding a mixture of raw bio-oil/ethanol (20 wt% of ethanol) in a two-step system: the first for thermal treatment of bio-oil at 500 °C, with pyrolytic lignin separation, and the second for the steam reforming of volatiles in a fluidized bed catalytic reactor at 700 °C. The properties of the catalysts were analyzed by N_2 adsorption–desorption, hydrogen chemisorption, inductively coupled plasma atomic emission mass spectroscopy (Q-ICP-MS), X-ray diffraction spectroscopy (XRD) and temperature programmed reduction (TPR). The coke deposited on the deactivated catalysts was quantified by temperature programmed oxidation (TPO). Both calcination and reduction temperatures have a significant effect on the amount and nature of the active metal dispersed on the support and they play an important role on the activity and stability of the catalyst throughout the reforming reaction. The catalyst calcined at 550 °C and reduced at 700 °C yielded the highest values of bio-oil conversion and hydrogen yield and were the most stable of the tested catalysts over 4 h reaction.

© 2013 Elsevier B.V. All rights reserved.

1. Introduction

The steam reforming of bio-oil is considered as an interesting route for hydrogen production with low CO_2 emission [1–4]. This process avoids the costs of bio-oil pre-treatment required for other routes of exploitation, which is very interesting for the bio-oil valorization on a large scale. The bio-oil water content (20–35 wt%) is suitable for the steam reforming since it avoids the costly dehydration required for bio-oil valorization as a fuel. The technology of bio-oil production by flash pyrolysis of lignocellulosic biomass is already mature [5–8].

Nevertheless, the raw bio-oil tends to re-polymerize to form a carbonaceous solid (pyrolytic lignin) which creates problems for the reactor operation and also for catalyst deactivation. Consequently, in most of the studies of bio-oil reforming, its aqueous fraction is valorized, usually with Ni supported catalysts [9–14]. This fraction, which is separated by adding water to raw bio-oil [15], has a lower content of the compounds that cause the pyrolytic lignin deposition. The addition of La_2O_3 as promoter contributes to decreasing catalyst deactivation and enhances the selectivity to hydrogen in the steam reforming of bio-oil aqueous fraction [16].

In order to reform the raw bio-oil with the pyrolytic lignin deposition on the catalyst being attenuated, different strategies have been used: (i) the prior separation of pyrolytic lignin which is formed by vaporizing the bio-oil [17]; (ii) the operation in reforming–regeneration cycles (by pyrolytic lignin combustion) [18,19]; (iii) the co-feeding of methanol [20]; and (iv) the operation with two reactors in line. Wu et al. [21] used in a first reactor a low-cost catalyst (dolomite) on which the pyrolytic lignin was deposited. van Rossum et al. [22] used a fluidized bed with sand for a primary gasification at low temperature and the volatiles were reformed in a second reactor. Remiro [23] retained the pyrolytic lignin in a U-shaped steel tube (thermal treatment reactor) and the remaining volatiles were reformed in a fluidized bed reactor. Some of these strategies were also useful for the raw bio-oil valorization by cracking over acid catalysts for obtaining olefins, aromatics and automotive fuels [24–29].

Several methods have been used in the literature for synthesizing the Ni catalysts, supported on α- or γ-Al_2O_3 (alone or promoted with La_2O_3), such as co-precipitation [11,30–32], sol–gel [33], surfactant assisted method [32] and the incipient wetness impregnation [16,34–40], which has been the most widely used. Moreover, a wide range of calcination/reduction temperatures (between 500 °C and 850 °C) has been used. It was found that the

* Corresponding author. Tel.: +34 946 015 361; fax: +34 946 013 500.
E-mail address: beatriz.valle@ehu.es (B. Valle).

0926-3373/$ – see front matter © 2013 Elsevier B.V. All rights reserved.
http://dx.doi.org/10.1016/j.apcatb.2013.09.022

Nomenclature

C_C	coke content (wt%)
F_i	molar flow rate of bio-oil or ethanol (C units)
G_{C1}HSV	Gas hourly space velocity, defined in equivalent CH_4 units (h^{-1})
Y_{H_2}	hydrogen yield for the reforming step, expressed as percentage of the stoichiometric maximum (%)
Y_C	coke yield in units of C fed, g coke (g C fed)$^{-1}$ (wt%)
Y_i	*i* carbonaceous product yield, in units of carbon fed, mol *i* (mol C fed)$^{-1}$ (%)
S/C	steam to carbon ratio in the feed to catalytic reactor
X_i	bio-oil or ethanol conversion

synthesis and preparation conditions had a direct influence on the kinetic behavior, because of their different metal surface and Ni dispersion.

This paper studies the influence of calcination and reduction temperatures on the Ni/La_2O_3–αAl_2O_3 catalyst properties and, consequently, on its activity and stability in the steam reforming of raw bio-oil. The objective is to define the optimum preparation conditions for reforming a mixture of raw bio-oil and ethanol in a reaction system with two steps in series (thermal-catalytic). In a previous work in which the reforming of bio-oil aqueous fraction was studied, the notable effect of La_2O_3 addition for improving the catalyst stability was proven [16]. The co-feeding of ethanol with raw bio-oil is interesting for several reasons: (i) ethanol can be used instead of methanol to stabilize the raw bio-oil during its storage, (ii) it contributes to increasing the H/C ratio of the feed, and therefore the pyrolytic lignin deposition decreases and (iii) it can be obtained by hydrolysis–fermentation of lignocellulosic biomass, thus contributing to the sustainability of the overall process for hydrogen production.

2. Experimental

2.1. Synthesis and preparation of Ni/La_2O_3–αAl_2O_3 catalysts

The catalyst was synthesized *via* the incipient wetness technique by using α-Al_2O_3 (supplied by Derivados del Fluor, Castro Urdiales, Spain) as support. Prior to Ni loading, the Al_2O_3 support was modified with La_2O_3 by impregnation with an aqueous solution of $La(NO_3)_3{\cdot}6H_2O$ (Alfa Aesar, 99%), under vacuum at 70 °C. The La-modified support was dried at 100 °C for 24 h and calcined at 900 °C for 3 h. Subsequently, Ni was added by impregnation with $Ni(NO_3)_2{\cdot}6H_2O$. After drying at 110 °C for 24 h, the final calcination was carried out for 3 h at three different temperatures (550, 700 and 850 °C).

All the catalysts were prepared with nominal contents of 10 wt% of Ni and 9 wt% of La_2O_3. This Ni content was determined as optimal in a previous work [41] which studied the effect of Ni content on the catalyst activity and stability for ethanol steam reforming. The La_2O_3 loading (9 wt%) was selected on the basis of many previous studies on reforming of oxygenates [30,36,38], bio-oil aqueous fraction [16], raw bio-oil [36], ethanol [33,35,42], and its mixtures with glycerol [39] and glycerine [40].

The catalysts calcined at different temperatures were sieved (150–250 μm) and mixed with an inert solid (carborundum, 37 μm) in catalyst/inert mass ratio of 1/4 and were reduced in the reactor itself, under H_2/He flow with 5% (v/v) of H_2, for 2 h at 700 °C or at 850 °C, prior to the reforming reactions. The prepared Ni/La_2O_3–αAl_2O_3 catalysts were denoted as $NiLa_{T1-T2}$, where T1 and T2 are the calcination and the reduction temperature, respectively.

2.2. Characterization of the catalysts

The physical properties of the catalysts (BET surface area and pore volume) were quantified from the N_2 adsorption–desorption isotherms, obtained by using a Quantachrome IQ2 analyzer. This device was also used for hydrogen chemisorption measurements for quantifying the metal dispersion and the specific metal surface (m^2/g_{metal}) with the following procedure: after initial evacuation step, the metal phase was reduced for 6 h with H_2 flow, following a heating ramp up to 700 °C or 850 °C. Then impurities were removed from the catalyst surface (evacuation with He) and analyses were carried out at 35 °C. The irreversibly chemisorbed H_2 (adsorbed on the metal surface) was determined by the method of double isotherm, considering an irreversible adsorption on the metal phase, a reversible adsorption on the support and assuming the adsorption stoichiometry of H:Ni = 1:1 [32]. The actual metal contents in the catalysts, 9.84 wt% Ni and 7.89 wt% La_2O_3, measured by inductively coupled plasma quadrupole mass spectroscopy (Q-ICP-MS), were very similar to the nominal contents. Moreover, these average values were obtained with very low standard deviation (experimental error) and thereby, the reproducibility of the synthesis method is checked.

The X-ray diffraction (XRD) analysis of the catalysts was performed on a Bruker D8 Advance diffractometer with a $CuK_{\alpha 1}$ ($\lambda = 0.154056$ nm) radiation. The reduced catalysts were transferred to the XRD apparatus in a sealed container. The average NiO particle size (for calcined catalysts) and the Ni^0 particle size (for calcined–reduced catalysts) were determined by applying the Scherrer formula to their corresponding peaks.

Temperature programmed reduction (TPR) analyses were carried out for determining the reduction temperature of the different metallic phases of the catalysts. These tests were conducted at atmospheric pressure by using a Micromeritics AutoChem II 2920. For each experiment, 100–200 mg of sample was loaded in a U-shaped quartz reactor tube and placed into the sample port, located inside a heater. The temperature of the sample bed was raised from ambient up to 950 °C at a heating rate of 10 °C/min.

The temperature programmed oxidation (TPO) analysis of the coke deposited on the catalysts deactivated in the steam reforming reactions was conducted by combustion with air in a TA Instruments Q5000 IR thermobalance, coupled to a mass spectrometer Thermostar Balzers Instrument for monitoring the signal corresponding to CO_2. These TPO analysis were conducted under air in excess conditions, thus the CO concentration in the outlet stream is negligible.

2.3. Reaction equipment for the steam reforming

The reaction equipment has been previously described in detail for the steam reforming of aqueous bio-oil [16] and it consists of two reactors in-line (Fig. 1). The first reactor (thermal treatment of the bio-oil/ethanol feed) is a U-shaped tube (S-316 stainless steel, 5/8″ internal diameter) which retains the carbonaceous solid (pyrolytic lignin) formed by re-polymerization of certain bio-oil oxygenates (mainly those derived from the pyrolysis of biomass lignin). The bio-oil/ethanol mixture (raw bio-oil stabilized with 20 wt% of ethanol) was fed as droplets that were introduced into the first reactor by the carrier flow (He). The feeding rate (0.1 ml/min) was controlled by an injection pump (Harvard Apparatus 22) and the water flow-rate was 0.31 ml/min (by 307 Gilson pump). The volatile stream leaving the thermal step was subsequently transformed (by catalytic steam reforming) in a second unit (fluidized bed reactor). The controlled deposition of pyrolytic lignin in a specific thermal step prior to the catalytic reactor minimizes the operating problems caused by this deposition and attenuates the catalyst deactivation. This fact was previously verified for the

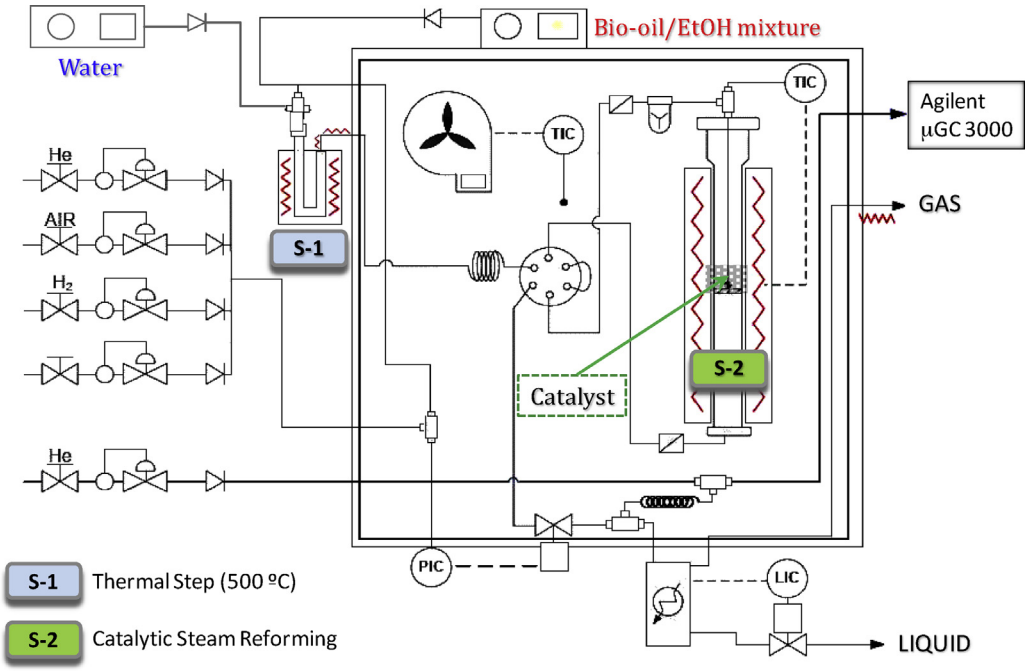

Fig. 1. Two-step (thermal-catalytic) reaction equipment for steam reforming of raw bio-oil stabilized with 20 wt% of ethanol.

catalytic conversion of raw bio-oil into hydrocarbons [25,26]. Furthermore, the fluidized bed reactor has proven to have advantages for the bio-oil reforming [11,20] because it guarantees the isothermicity and enhances the bed uniformity for both deactivation and reforming of coke precursors, and therefore the catalyst deactivation is attenuated [43]. In addition, the fluidized bed reactor is interesting for increasing scale because of its ability to work with catalyst circulation in a reactor–regenerator system and because it allows the *in situ* use of CO_2 adsorbents [44]. The hydrodynamic properties of the reactor, which determines the feed flow-rate, were established in a previous paper [41] by cold hydrodynamic studies, ensuring the fluidization of the catalyst + carborundum bed. By comparing the mass of the spent catalyst + carborundum bed with the initial mass of the bed, it was found that attrition is negligible. The coke deposited on the spent catalyst was considered for this quantification.

The on-line analysis of the reforming products was carried out continuously (more representative and steady than discontinuous sampling) with a gas chromatograph (Agilent Micro GC 3000) provided with four analytical modules for the analysis of: (1) permanent gases (O_2, H_2, CO, and CH_4) with 5A molecular sieve capillary column; (2) light oxygenates (C_{2-}), CO_2 and water, with Plot Q capillary column; (3) C_2–C_4 hydrocarbons, with alumina capillary column; (4) oxygenated compounds (C_{2+}) with Stabilwax type column.

Prior to each reforming reaction, the catalysts (1.3 g) were reduced *in situ* for 2 h under H_2–He flow (5% (v/v) of H_2) by following a temperature ramp of 10 °C/min from ambient up to 700 °C or 850 °C. The reforming conditions were: thermal step, 500 °C; catalytic steam reforming, 700 °C; steam-to-carbon ratio (S/C) at thermal step inlet, 6; space-time, 0.27 $g_{catalyst}h(g_{bio\text{-}oil+EtOH})^{-1}$; $G_{C1}HSV$, 13,800 h^{-1} (at reaction temperature, in CH_4 equivalent units). In order to have S/C = 6 at the first step inlet, water was fed along with the bio-oil/ethanol mixture at the flow-rate corresponding to this ratio, which leads to a value of S/C = 7.5 at the entrance of fluidized bed reactor. This difference is due to the deposition of pyrolytic lignin in the first thermal reactor, which diminishes the C content in the bio-oil flow-rate that enters the fluidized reactor. These operating conditions were established as suitable considering previous results of steam reforming of bio-oil aqueous fraction [16], raw bio-oil [23] and ethanol [41] in order to achieve a high yield of H_2 while maintaining the catalyst stability. 700 °C is a suitable temperature to attenuate coke deposition on the catalyst because the gasification of coke precursors is remarkable at this temperature. For both feeds of bio-oil and ethanol, which are valorized together in this paper, the suitable S/C ratio at the fluidized reactor inlet is 7.5 (6 at the inlet of the first reactor). In order to compare the catalysts in this paper all the experiments were performed under these conditions previously identified as suitable.

2.4. Feed characteristics

The raw bio-oil was obtained by flash pyrolysis of pine sawdust at 480 °C in a semi-industrial demonstration plant, located in Ikerlan-IK4 technology center (Alava, Spain), with a biomass feeding capacity of 25 kg/h [45]. This plant was developed based on the results obtained in a laboratory plant (120 g/h) at the University of the Basque Country [46,47]. The raw bio-oil composition was determined by GC/MS analyser (Shimadzu QP2010S device) and it is shown in Table 1, on a water-free basis. The corresponding molecular formula ($C_{3.5}H_{6.1}O_{3.3}$) was estimated from the composition results obtained by GC/MS and it was confirmed by elemental analysis (Leco CHN-932 analyzer and ultra-microbalance Sartorious M2P). The bio-oil water content, determined by Karl Ficher valorization (KF Titrino Plus 870), was 35 wt% and its average molecular weight, determined by Gel Permeation Chromatography (GPC) (Waters 616), was 886 g/mol. The ethanol to be mixed with the raw bio-oil for obtaining the bio-oil/ethanol feed was supplied by Panreac (96% (v/v)).

2.5. Reaction indices

The bio-oil steam reforming proceeds according to reforming reactions of oxygenated organic compounds ($C_nH_mO_k$), Eq. (1), followed by water-gas-shift reaction (WGS), Eq. (2):

$$C_nH_mO_k + (n-k)H_2O \rightarrow nCO + (n+(m/2)-k)H_2 \quad (1)$$

Table 1
Composition (wt%) of the raw bio-oil.

Compound/group	wt%
Acetic acid	10.2
Acetone	0.1
1-Hydroxy-2-propanone	6.9
1-Hydroxy-2-butanone	3.3
Hydroxyacetaldehyde	16.8
Methanol	1.9
Levoglucosane	22.5
Other ketones	
Linear	1.4
Cyclic	1.9
Other acids	7.4
Other alcohols	1.8
Other aldehydes	5.3
Esters	4.9
Eters	1.9
Phenols	6.5
Others	5.0
Non-identified	2.2

$$CO + H_2O \leftrightarrow CO_2 + H_2 \quad (2)$$

Ethanol can be efficiently converted into hydrogen by means of its steam reforming reaction:

$$CH_3CH_2OH + 3H_2O \rightarrow 2CO_2 + 6H_2 \quad (3)$$

In addition to the bio-oil and ethanol reforming, secondary reactions such as thermal and catalytic decomposition, decarbonylation and methanation should be considered. These reactions lead to the formation of by-products (CH_4 and light hydrocarbons, mainly ethylene and ethane) in the operating conditions studied. Other reactions involving formation and development of carbonaceous structures (coke) on the catalyst must also be considered.

The conversion of bio-oil and ethanol in the mixture fed are individually calculated from their molar flowrates at the inlet and outlet (un-reacted bio-oil or ethanol) of the catalytic reactor, according to:

$$X_i = \frac{F_{i,\text{inlet}} - F_{i,\text{outlet}}}{F_{i,\text{inlet}}} \quad (4)$$

where F_i are referred to the C units contained in the bio-oil or ethanol.

The bio-oil molar flowrate at catalytic reactor inlet ($F_{\text{bio-oil,inlet}}$) is determined by a mass balance, taking into account that 5.5 wt% of oxygenates in the raw bio-oil are retained as pyrolytic lignin in the thermal treatment (at 500 °C) of the mixture of raw bio-oil ($C_{3.5}H_{6.1}O_{3.3}$) and ethanol (C_2H_6O). This lignin has $C_{7.7}H_{3.0}O_{0.3}$ as elemental composition (quantified by elemental analysis). Consequently, the composition of the treated bio-oil that enters the fluidized bed reforming reactor is $C_{3.2}H_{6.2}O_{3.5}$ and thus the maximum H_2 yield (stoichiometric) is 1.89 mol H_2/mol C in the treated bio-oil (1.93 mol H_2/mol C in the raw bio-oil fed to the reaction system). Therefore, the thermal treatment that facilitates the reforming reaction has the disadvantage of reducing by 2.1% the maximum hydrogen yield. However, the pyrolytic lignin deposited can be valorized by treatments similar to those developed for the lignin derived from processing pulp [48].

The bio-oil molar flowrate at reactor outlet ($F_{\text{bio-oil,outlet}}$) is calculated from the molar fraction of oxygenates (analyzed by microGC and by GC/MS) and the total number of moles at the reactor outlet, determined by mass balance for the catalytic reactor.

The H_2 yield is calculated as a percentage of the stoichiometric potential, taking into account the contribution of both reactants (bio-oil and ethanol):

$$Y_{H_2} = \frac{\text{molar flow of } H_2 \text{ obtained}}{(1.89 \times F_{\text{bio-oil,inlet}} + 3 \times F_{\text{EtOH,inlet}})} \times 100 \quad (5)$$

Table 2
Physical properties of Ni/La_2O_3–αAl_2O_3 catalysts calcined at different temperatures.

Catalyst	BET surface area (m^2/g)	Pore volume (cm^3/g)	NiO size (nm)[a]
$NiLa_{550}$	33.9	0.167	10.0
$NiLa_{700}$	34.8	0.171	18.6
$NiLa_{850}$	36.2	0.181	–

[a] Derived from diffraction line in XRD corresponding to NiO (2 0 0) plane at 43.3°.

The yield of each carbon-containing byproduct (CO, CO_2, CH_4 and light hydrocarbons C_2–C_4) is quantified by:

$$Y_i = \frac{\text{molar flow of } i(\text{CO, CO}_2\text{, CH}_4\text{, HCs}) \text{ obtained}}{(F_{\text{bio-oil,inlet}} + F_{\text{EtOH,inlet}})} \times 100 \quad (6)$$

3. Results and discussion

3.1. Effect of calcination and reduction temperatures on the catalysts properties

The textural properties (BET surface area and pore volume) of the Ni/La_2O_3–αAl_2O_3 catalysts calcined at different temperatures are shown in Table 2, along with the NiO cluster size determined by XRD. The catalyst calcined at 550 °C ($NiLa_{550}$) has the lowest value of average NiO particle size, suggesting a higher metal dispersion. NiO is not detected at 850 °C as it combines to form $NiAl_2O_4$ due to the high temperature. There is a slight increase in the BET surface area as calcination temperature is higher (from 33.9 m^2/g at 550 °C up to 36.2 m^2/g at 850 °C). Consequently, the pore volume increases from 0.167 cm^3/g up to 0.181 cm^3/g. The effect of calcination temperature on the properties of the pores is very small and it may be explained by the structural changes of Ni and its linkages with the support as the calcination temperature is increased.

The temperature programmed reduction (TPR) profiles of the catalysts calcined at 550, 700 and 850 °C are reported in Fig. 2. The reduction profile of the $NiLa_{550}$ catalyst shows a wide asymmetric peak, (from temperatures of around 300 °C up to 800 °C) with a maximum at 570 °C. This suggests that more than one metal species contributes to the overall reduction of $NiLa_{550}$ catalyst and it evidences that temperature of around 800 °C is required to fully

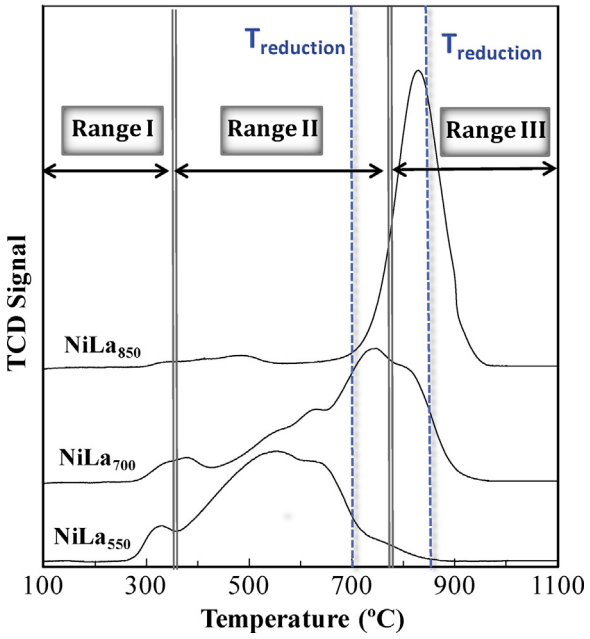

Fig. 2. Temperature programmed reduction (TPR) profiles of the catalysts calcined at 550, 700 and 850 °C.

reduce them. Fig. 2 also reveals that higher calcination temperatures enhance the distribution of reducible species (TPR profiles more homogeneous) although the peak shifts to higher temperatures. This result evidences the presence of Ni-containing phases which are less reducible (single peak at 840 °C for the catalyst calcined at 850 °C). Similar results with increasing the calcination temperature were obtained by Wang et al. [49] for Ni/La_2O_3–Al_2O_3 catalysts prepared by using the co-precipitation method.

Furthermore, the TPR profiles suggest that the Ni oxide precursors may be present in the catalysts in three different phases, which reduce in specific temperature ranges (I, II and III). The highest peak is assigned to reduction of the prevailing metal phase. The H_2 consumption in the range I (280–350 °C) is attributed to the bulk NiO reduction [50,51]. The peaks in the range II (350–780 °C) are attributed to the reduction of NiO_x surface phase which is highly dispersed and interacts strongly with the support [50,52]. Vogelaar et al. [51] found a stoichiometry of $x = 1.6$ for this NiO_x phase, indicating an excess of oxygen in these surface compounds. The range III (>780 °C) is attributed to the Ni atoms which have migrated into the Al_2O_3 support to form $NiAl_2O_4$ [53,54]. According to Jin et al. [55] this spinel-type metal phase is very resistant to reduction and it is stable even at 900 °C. The TPR results (Fig. 2) reveal that bulk NiO crystals are present in low amounts (on the outer surface of the support) for all catalysts and that amorphous NiO species (range II) are the prevailing metal phases in the $NiLa_{550}$ catalyst (with a maximum at 570 °C). As the calcination temperature is higher, the amount of less-reducible species increases, with the prevailing metal phase in the $NiLa_{850}$ catalyst being $NiAl_2O_4$ spinel (whose reduction occurs at temperatures above 780 °C).

The XRD results of the calcined catalysts (Fig. 3a) show the presence of NiO phase (at $2\theta = 43°$ and 63°) and $NiAl_2O_4$ phase (at $2\theta = 19°$, 45° and 60°). The diffraction lines corresponding to reflection of Al_2O_3 phase are also shown. Similarly to other works [56,57] the presence of $LaAlO_3$ phase (La_2O_3 combined with α-Al_2O_3) is also detected. The diffraction lines corresponding to NiO phase become sharper as the calcination temperature is increased, which indicates some sintering of NiO crystallites, resulting in higher values of particle size (Table 2). Vos et al. [50] explained this effect by the presence of water vapor and acidic gases (coming from the nitrates decomposition) during the catalyst calcination, which led to larger Ni metal particles under more severe calcination conditions. The presence of NiO phase is not detected in the $NiLa_{850}$ catalyst and the peak corresponding to $NiAl_2O_4$ phase is higher (Fig. 3a). This suggests that the Ni in the catalyst combines with the Al_2O_3 to form spinel at calcination temperature of 850 °C, which corroborates the TPR results.

Based on the above TPR results (Fig. 2) which gave information about the temperature required for achieving full reduction of metal phases in the catalysts, the $NiLa_{550}$ catalyst was subsequently reduced at 700 °C, the $NiLa_{700}$ was reduced at both 700 °C and 850 °C (in order to analyze how the presence of non fully reduced species affects the catalytic behavior) and the $NiLa_{850}$ catalyst was reduced at 850 °C.

The XRD results corresponding to the catalysts calcined and reduced at different temperatures are shown in Fig. 3b, where the peaks corresponding to Ni^0 phase are identified. The presence of the same phases as in calcined samples ($NiAl_2O_4$, $LaAlO_3$ and Al_2O_3) can also be noticed.

Table 3 reports the metallic properties (cluster size, Ni surface and dispersion) determined by XRD and H_2 chemisorption of the catalysts calcined and reduced at different temperatures. The reduction degree of the catalysts (% of reduction) was also quantified from the TPR runs (Fig. 2), according to the method used by Ibrahim and Idem [32] and the results are included in Table 3. The $NiLa_{550–700}$ has the lowest Ni^0 crystallite size and the highest values of Ni^0 surface and dispersion. The values of Ni^0 surface show in general the same trend as Ni^0 dispersion, while the crystallite size follows an inverse trend. It is noteworthy that after reduction at 850 °C of the catalyst calcined at 700 °C, the catalyst ($NiLa_{700–850}$) has higher values of metal surface and dispersion compared to those obtained after reduction at 700 °C ($NiLa_{700–700}$), although the Ni^0 particle size is higher. Ni^0 dispersion value in the $NiLa_{700–850}$ (higher than that expected) could be caused by the higher temperature, as larger fraction of metal oxides is reduced (Fig. 2) and thereby, a higher Ni^0 surface is available, even though a higher temperature also promotes a slight metal sintering during reduction. The addition of La_2O_3 to αAl_2O_3 support improves NiO reduction and attenuates deactivation of the catalyst [58].

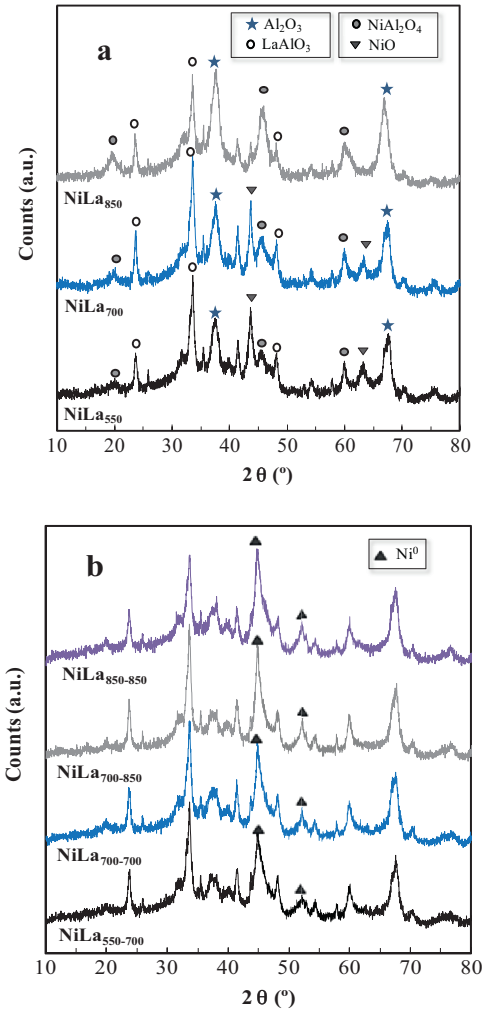

Fig. 3. XRD spectra of the calcined Ni/La_2O_3–αAl_2O_3 catalysts (a) and after reduction at 700 and 850 °C (b).

Table 3
Metallic properties of the Ni/La_2O_3–αAl_2O_3 catalysts calcined and reduced at different temperatures.

Catalyst	Ni^0 size (nm)[a]	Ni^0 surface area (m^2/g)	Dispersion Ni^0 (%)	Reduction (%)[b]
$NiLa_{550–700}$	4.9	5.3	8.6	87
$NiLa_{700–700}$	7.9	3.7	5.1	49
$NiLa_{700–850}$	9.2	4.0	5.6	92
$NiLa_{850–850}$	7.7	3.2	5.1	72

[a] Derived from diffraction line in XRD corresponding to Ni (2 0 0) plane at 51.6°.
[b] Measured *via* the convolution theory as the fraction of area under the TPR curve at reduction temperature with respect to the entire area.

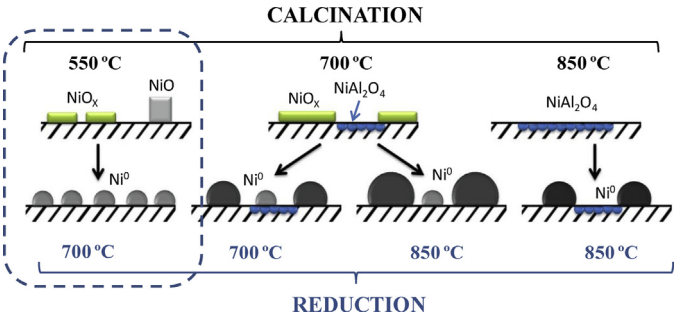

Fig. 4. Model for the reduction of $Ni/La_2O_3–\alpha Al_2O_3$ catalyst after different calcination temperatures.

Based on the afore-mentioned results, the increase in calcination temperature from 550 °C to 850 °C leads to the formation of larger clusters of Ni oxides, with higher interactions with the support and thereby, higher temperatures are required to reduce them (Fig. 4). The prevailing metal phases in the catalyst calcined at 550 °C are surface oxides (NiO_x), resulting in a catalyst with a homogeneous Ni^0 particle distribution and good dispersion after reduction at 700 °C. In order to set the optimum calcination/reduction conditions, the following order in the catalysts can be established based on the available metal surface (Table 3): $NiLa_{550–700} > NiLa_{700–850} > NiLa_{700–700} > NiLa_{850–850}$.

3.2. Kinetic behavior of the catalysts

3.2.1. Activity and stability of the catalysts

Fig. 5 shows the evolution with time on stream of conversion of the bio-oil (Fig. 5a) and ethanol (Fig. 5b) fed in the mixture for the catalysts prepared with different calcination/reduction temperatures. The evolution with time on stream of product yields is shown in Fig. 6 for H_2 (a), CO_2 (b), CO (c), CH_4 (d) and $C_2–C_4$ hydrocarbons (e). The CH_4 and $C_2–C_4$ hydrocarbons are formed by thermal cracking of bio-oil oxygenates [16].

The space-time used in these experiments ($0.27\ g_{catalyst}h(g_{bio\text{-}oil+EtOH})^{-1}$) is enough for attaining full conversion at zero time on stream (fresh catalyst) for all catalysts and no remarkable effects of calcination and/or reduction temperatures on initial conversions are observed (Fig. 5). Similarly, the yields at zero time on stream of H_2 (Fig. 6a), CO_2 (Fig. 6b), CO (Fig. 6c), CH_4 (Fig. 6d) and hydrocarbons (Fig. 6e) are almost independent of the calcination/reduction temperatures. Nevertheless, the evolution with time on stream of conversion and product yields reveals clear differences in the stability of the catalysts. The bio-oil conversion decreases from 1 to 0.65 after 4 h reaction (Fig. 5a) and the conversion of ethanol decreases from 1 to 0.88 (Fig. 5b) for the catalyst calcined and reduced at 850 °C ($NiLa_{850–850}$). On the other side, the $NiLa_{550–700}$ catalyst shows a very steady behavior with full conversion along 4 h reaction (Fig. 5). The catalysts that were calcined at 700 °C ($NiLa_{700–700}$ and $NiLa_{700–850}$) show an intermediate behavior in the bio-oil and ethanol conversion. A comparison of the decrease with time on stream of the conversion of bio-oil with that of ethanol shows that catalyst deactivation has a greater impact on the bio-oil reforming (Fig. 5a). This fact indicates that the steam reforming of bio-oil requires a higher catalyst activity than the ethanol reforming (Fig. 5b).

Concurrently with the conversion decrease, the H_2 yield decreases and the yield of by-products (CO, CH_4 and $C_2–C_4$ hydrocarbons) increases (Fig. 6). The H_2 yield gradually drops from 90% to 18% for the most unstable catalyst ($NiLa_{850–850}$) (Fig. 6a) and the yields of CO, CH_4 and hydrocarbons increase (Fig. 6c–e). The increase in CH_4 and CO yields is caused by the rapid loss of catalyst activity for the CH_4 reforming reaction and for the WGS reaction,

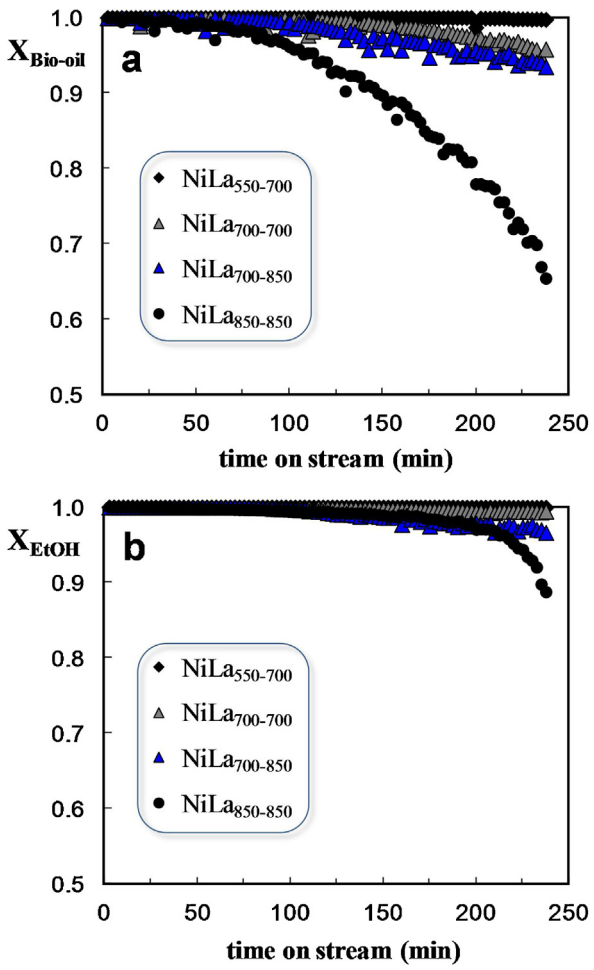

Fig. 5. Evolution with time on stream of conversion of bio-oil (a) and ethanol (b) for $Ni/La_2O_3–\alpha Al_2O_3$ catalysts. Conditions: 700 °C; G_{C1} HSV = 13,800 h^{-1}; S/C = 6; $0.27\ g_{catalyst}h(g_{bio\text{-}oil+EtOH})^{-1}$.

while its activity for reforming $C_2–C_4$ hydrocarbons remains constant for 70 min. The yields of these byproducts have a maximum value because of the decrease in conversion. On the other side, the $NiLa_{550–700}$ catalyst shows a very steady behavior, with a slight decrease in H_2 yield from 94% to 87% (Fig. 6a) and a slight increase in the yields of CO and CH_4 (Fig. 6c and d) in 4 h reaction, while the $C_2–C_4$ hydrocarbons yield is negligible.

The catalysts that were calcined at 700 °C ($NiLa_{700–700}$ and $NiLa_{700–850}$) have an intermediate behavior in the evolution of product yields compared to the catalysts calcined at 550 °C and 850 °C. The H_2 yield obtained with the catalyst reduced at 850 °C ($NiLa_{700–850}$) is slightly higher than that obtained with the sample reduced at 700 °C ($NiLa_{700–700}$) (Fig. 6a). This is explained by the higher and better dispersed metal surface available for reforming reaction (Table 3), consequence of the higher reduction temperature which allows nearly full reduction of all Ni species. Nevertheless, the H_2 yield obtained with $NiLa_{700–850}$ is not as high as that expected, considering the higher values of Ni^0 dispersion, metal surface and % of reduction compared to $NiLa_{700–700}$ (Table 3). This fact suggests that the Ni^0 coming from reduction of spinel ($NiAl_2O_4$) is less active than that coming from Ni oxides. This hypothesis is confirmed by the results obtained with the catalyst calcined at 850 °C ($NiLa_{850–850}$), which undergoes a sharp decrease in conversion and product yields. This behavior is caused by the lower activity of the Ni^0 coming from spinel (prevailing phase in the $NiLa_{850–850}$ catalyst, Fig. 2), so that the catalyst deactivates

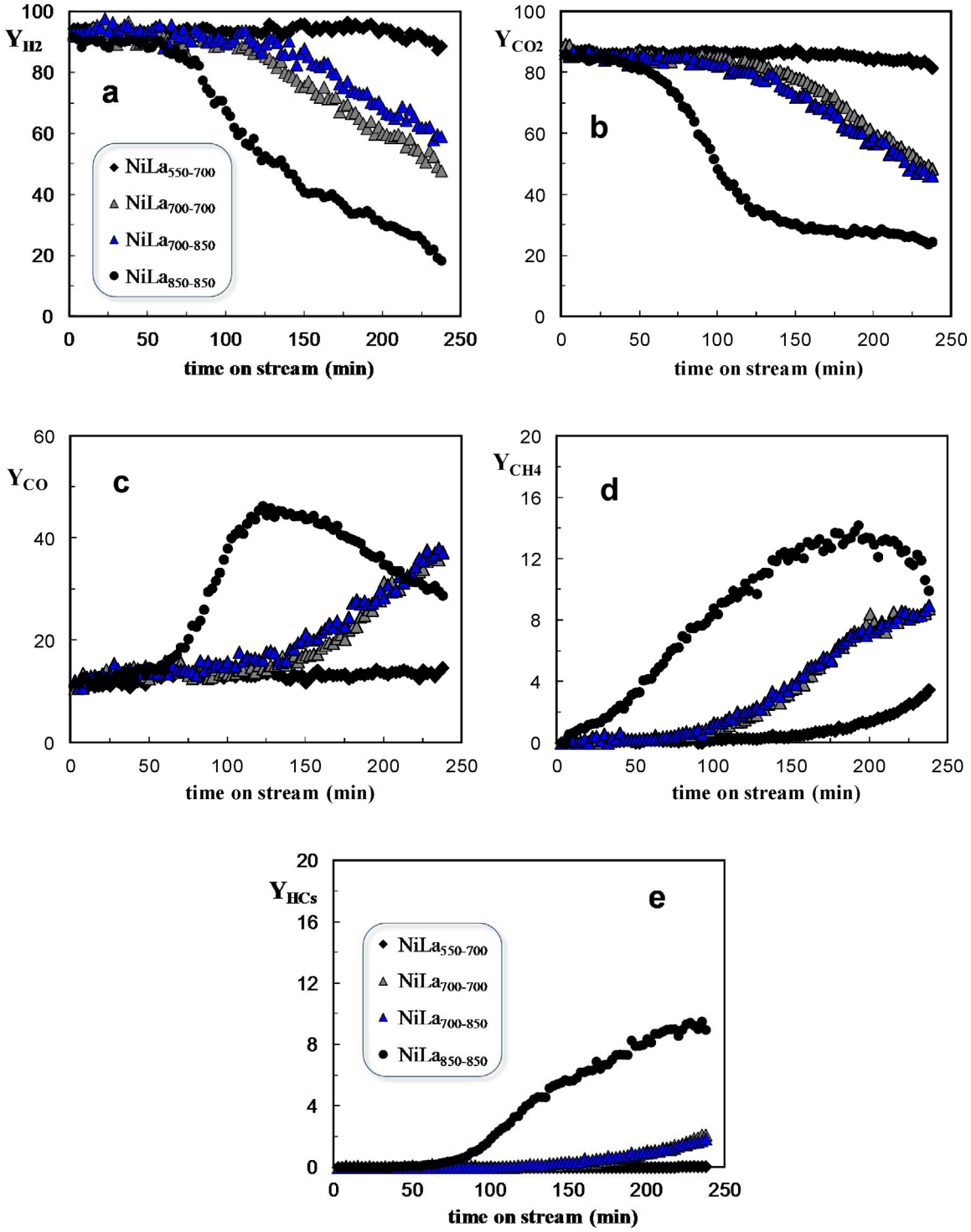

Fig. 6. Evolution with time on stream of the yield of H_2 (a), CO_2 (b), CO (c), CH_4 (d) and HCs (e) for $Ni/La_2O_3–\alpha Al_2O_3$ catalysts. Conditions: 700 °C; $G_{C1}HSV = 13{,}800\ h^{-1}$; S/C = 6; 0.27 $g_{catalyst}\,h(g_{bio\text{-}oil+EtOH})^{-1}$.

more rapidly as it operates far from the thermodynamic regime. Moreover, this catalyst is more affected by both causes of deactivation (coke deposition and Ni sintering), as it is discussed in the following section.

The above-shown results confirm that a lower calcination temperature of the catalyst (550 °C) improves its performance for hydrogen production by steam reforming of the bio-oil/ethanol mixture, because the formation of CO, CH_4 and light hydrocarbons (consequence of catalyst deactivation) is attenuated.

3.2.2. Cause of catalyst deactivation

Possible causes of catalyst deactivation in the steam reforming of oxygenates are coke deposition, which blocks the metal active sites, and metal sintering, which increases the average Ni particle size. Both effects decrease the metal surface accessible to reactants [59]. Table 4 shows the yield of coke (by C unit fed, Y_C, wt%) and the coke content deposited on the catalysts (C_C, wt%) after reforming reactions corresponding to Figs. 5 and 6. The coke content on the inert carborundum (by TPO analysis) was found negligible, which

Table 4
Coke content deposited on the catalysts (C_C, wt%), yield of coke by C unit fed (Y_C, wt%) and average nickel particle size after steam reforming reaction: 4 h at 700 °C, S/C = 6, 0.27 $g_{catalyst}h(g_{bio\text{-}oil+EtOH})^{-1}$.

Catalyst	C_C (wt%)	Y_C (wt%)	Ni^0 size (nm)	
			Fresh	Deactivated
$NiLa_{550-700}$	1.1	0.19	4.9	12.3
$NiLa_{700-700}$	2.4	0.40	7.9	22.7
$NiLa_{700-850}$	5.6	0.94	9.2	25.3
$NiLa_{850-850}$	4.1	0.79	7.7	30.5

demonstrates the effectiveness of the prior thermal treatment step to retain the pyrolytic lignin, responsible of the thermal origin coke that would deposit both on the catalyst and on carborundum. The average Ni particle size (determined by XRD) for fresh and deactivated catalysts (after 4 h reaction) is also shown. These results reveal that the cause of catalyst deactivation is a combination of both sintering and coke formation.

In general, as the calcination and reduction temperatures are increased the coke deposition is greater. This is related to the formation of hydrocarbons as byproducts, which are considered precursors of coke formation by reactions of dehydrogenation, aromatization and condensation [60,61]. However, the coke deposition in the catalyst calcined and reduced at 850 °C ($NiLa_{850-850}$) is lower than the $NiLa_{700-850}$ catalyst, suggesting that the active sites of the $NiLa_{850-850}$ catalyst have lower activity for both the reforming reaction and the development of carbonaceous structures from coke precursors. Concerning the other possible cause of deactivation (metal sintering), a higher Ni particle size is observed in all catalysts after 4 h reaction (Table 4), with the most significant increase for the $NiLa_{850-850}$ catalyst. This more severe sintering results in a noticeable deactivation (Figs. 5 and 6) and it is caused by the presence of $NiAl_2O_4$ spinel particles (prevailing in this catalyst) reducing to Ni^0 species that are more liable to sintering.

The results of coke content and Ni^0 particle size of the catalysts calcined at 700 °C and reduced at 700 °C ($NiLa_{700-700}$) and at 850 °C ($NiLa_{700-850}$) reveal that the sintering severity is similar in both catalysts, although the coke content of the $NiLa_{700-850}$ catalyst is above double that of the $NiLa_{700-700}$ catalyst. This effect is caused by the presence of larger Ni^0 particles (Table 3) which enhances formation and growth of carbon whiskers [59]. The catalysts reduced at 850 °C after calcination at different temperatures ($NiLa_{700-850}$ and $NiLa_{850-850}$) show different deactivation results (Figs. 5 and 6), with coke contents being similar but sintering severity very different (Table 4). These results evidence that Ni sintering causes a greater impact than the coke deposition on the loss of catalyst activity. The catalyst that undergoes less coke deposition and a lower sintering is the sample calcined at 550 °C and subsequently reduced at 700 °C ($NiLa_{550-700}$), which is in total agreement with the lowest deactivation observed in Figs. 5 and 6.

4. Conclusions

The steam reforming of raw bio-oil mixed with ethanol in a two-step system (for separating the pyrolytic lignin and reforming *in-line* of the volatiles in a fluidized bed reactor) over $Ni/La_2O_3–\alpha Al_2O_3$ catalyst performs well for hydrogen production from lignocellulosic biomass.

The calcination and reduction temperatures of the catalyst have a great influence on its activity and stability, because not only a high and well dispersed Ni^0 metal surface (available for reforming reaction) is important, but the origin of this Ni^0 (oxide precursors) has also proven to be a key factor.

As the calcination temperature is higher, the catalyst reducibility diminishes due to the formation of $NiAl_2O_4$, which has stronger interaction with the support than NiO_x oxides. Calcination temperatures below 700 °C avoid the formation of clusters, by separating the Ni crystals and thereby, metal dispersion and reducibility are enhanced. The presence of $NiAl_2O_4$ spinel-type structures in the calcined catalysts favors the formation of larger (and less active) Ni^0 crystallites after reduction. These Ni^0 particles are also more liable to sintering (main cause of deactivation) in the steam reforming reaction of the raw bio-oil and ethanol mixture.

Consequently, the catalyst calcined at 550 °C and reduced at 700 °C has the most suitable structural features (the greatest metal surface with the best dispersion). The calcination at 550 °C minimizes the formation of $NiAl_2O_4$ spinel and produces a larger amount of highly dispersed Ni oxides, which reduce to form highly dispersed Ni^0 nanoparticles that are more resistant to sintering. These better structural features lead to a higher reforming activity and a more steady hydrogen production in the raw bio-oil/ethanol steam reforming, because of the catalyst ability to avoid both coke formation on its surface (small and well dispersed nickel crystallites) and metal sintering.

Acknowledgements

This work was carried out with the financial support of the Department of Education Universities and Investigation of the Basque Government (Project GIC07/24-IT-220-07), the University of the Basque Country (UFI 11/39 UPV/EHU) and the Ministry of Science and Innovation of the Spanish Government (Project CTQ2009-13428/PPQ). B. Aramburu thanks the University of the Basque Country for his PhD grant (UPV/EHU2011).

References

[1] S. Czernik, R. French, C. Feik, E. Chornet, Ind. Eng. Chem. Res. 41 (2002) 4209–4215.
[2] S.A. Chattanarthan, S. Adhikari, N. Abdoulmoumine, Renew. Sust. Energy Rev. 16 (2012) 2366–2372.
[3] R. Trane, S. Dahl, M.S. Skjøth-Rasmussen, A.D. Jensen, Int. J. Hydrogen Energy 37 (2012) 6447–6472.
[4] A.A. Lemonidou, P. Kechagiopoulos, E. Heracleous, S. Voutetakis, The Role of Catalysis for the Sustainable Production of Biofuels and Bio-chemicals, Elsevier, Amsterdam, 2013, pp. 467 (Chapter 14).
[5] A. Oasmaa, Y. Solantausta, V. Arpiainen, E. Kuoppala, K. Sipilä, Energy Fuels 24 (2010) 1380–1388.
[6] E. Butler, G. Devlin, D. Meier, K. McDonnell, Renew. Sust. Energy Rev. 15 (2011) 4171–4182.
[7] A.V. Bridgwater, Biomass Bioenergy 38 (2012) 68–94.
[8] D. Meier, B. van de Beld, A.V. Bridgwater, D.C. Elliott, A. Oasmaa, F. Preto, Renew. Sust. Energy Rev. 20 (2013) 619–641.
[9] P.N. Kechagiopoulos, S.S. Voutetakis, A.A. Lemonidou, I.A. Vasalos, Energy Fuels 20 (2006) 2155–2163.
[10] P.N. Kechagiopoulos, S.S. Voutetakis, A.A. Lemonidou, I.A. Vasalos, Ind. Eng. Chem. Res. 48 (2009) 1400–1408.
[11] J.A. Medrano, M. Oliva, J. Ruiz, L. García, J. Arauzo, Energy 36 (2011) 2215–2224.
[12] P.J. Ortiz-Toral, J. Satrio, R.C. Brown, B.H. Shanks, Energy Fuels 25 (2011) 3289–3297.
[13] S. Liu, M. Chen, L. Chu, Z. Yang, C. Zhu, J. Wang, M. Chen, Int. J. Hydrogen Energy 38 (2013) 3948–3955.
[14] J. Remón, J.A. Medrano, F. Bimbela, L. García, J. Arauzo, Appl. Catal. B 132 (2013) 433–444.
[15] A. Oasmaa, S. Cernik, Energy Fuels 13 (1999) 914–921.
[16] B. Valle, A. Remiro, A.T. Aguayo, J. Bilbao, A.G. Gayubo, Int. J. Hydrogen Energy 38 (2013) 1307–1318.
[17] Z. Wang, Y. Pan, T. Dong, X. Zhu, T. Kan, L. Yuan, Y. Torimoto, M. Sadakata, Q. Li, Appl. Catal. A 320 (2007) 24–34.
[18] E.E. Iojoiu, M.E. Domine, T. Davidian, N. Guilhaume, C. Mirodatos, Appl. Catal. A 323 (2007) 147–161.
[19] M.E. Domine, E.E. Iojoiu, T. Davidian, N. Guilhaume, C. Mirodatos, Catal. Today 133 (2008) 565–573.
[20] S. Czernik, R. Evans, R. French, Catal. Today 129 (2007) 265–268.
[21] C. Wu, Q. Hunag, M. Sui, Y. Yan, F. Wang, Fuel Process. Technol. 89 (2008) 1306–1316.
[22] G. van Rossum, S.R.A. Kerrsten, W.P.M. van Swaaij, Ind. Eng. Chem. Res. 48 (2009) 5857–5866.
[23] A. Remiro, Hydrogen Production by Steam Reforming of Bio-oil. Integration of Thermal, Catalytic and CO Capture Steps in the Process, University of Basque Country UPV/EHU, Bilbao, Spain, 2012 (Ph.D. Thesis).

[24] A.G. Gayubo, B. Valle, A.T. Aguayo, M. Olazar, J. Bilbao, Energy Fuels 23 (2009) 4129–4136.
[25] A.G. Gayubo, B. Valle, A.T. Aguayo, M. Olazar, J. Bilbao, Ind. Eng. Chem. Res. 49 (2010) 123–131.
[26] B. Valle, A.G. Gayubo, A.T. Aguayo, M. Olazar, J. Bilbao, Energy Fuels 24 (2010) 2060–2070.
[27] M. Bertero, G. de la Puente, U. Sedran, Energy Fuels 25 (2011) 1267–1275.
[28] M. Bertero, G. de la Puente, U. Sedran, Fuel 95 (2012) 263–271.
[29] M. Bertero, U. Sedran, Bioresour. Technol. 135 (2013) 644–651.
[30] J.R. Galdamez, L. García, R. Bilbao, Energy Fuels 19 (2005) 1133–1142.
[31] F. Bimbela, M. Oliva, J. Ruiz, L. García, J. Arauzo, J. Anal. Appl. Pyrolysis 85 (2009) 204–213.
[32] H.H. Ibrahim, R.O. Idem, Energy Fuels 22 (2008) 878–891.
[33] R. Carrera Cerritos, R. Fuentes Ramirez, A.F. Aguilera Alvarado, J.M. Martínez Rosales, T. Viveros García, I.R. Galindo Esquivel, Ind. Eng. Chem. Res. 50 (2011) 2576–2584.
[34] F. Seyedeyn-Azad, E. Salehi, J. Abedi, T. Harding, Fuel Process. Technol. 92 (2011) 563–569.
[35] M.C. Sánchez-Sánchez, R.M. Navarro, J.L.G. Fierro, Int. J. Hydrogen Energy 32 (2007) 1462–1471.
[36] T. Davidian, N. Guilhaume, E. Iojoiu, H. Provendier, C. Mirodatos, Appl. Catal. B 73 (2007) 116–127.
[37] A.C. Basagiannis, X.E. Verykios, Appl. Catal. A 308 (2006) 182–193.
[38] A. Iriondo, J.F. Cambra, V.L. Barrio, M.B. Guemez, P.L. Arias, M.C. Sánchez-Sánchez, R.M. Navarro, J.L.G. Fierro, Appl. Catal. B 106 (2011) 83–93.
[39] M. El Doukkali, A. Iriondo, P.L. Arias, J.F. Cambra, I. Gandarias, V.L. Barrio, Int. J. Hydrogen Energy 37 (2012) 8298–8309.
[40] A. Iriondo, V.L. Barrio, M. El Doukkali, J.F. Cambra, M.B. Güemez, J. Requies, P.L. Arias, M.C. Sánchez-Sánchez, R. Navarro, J.L.G. Fierro, Int. J. Hydrogen Energy 37 (2012) 2028–2036.
[41] J. Vicente, Catalysts and Operating Conditions for the Production of Hydrogen by the Steam Reforming of Dimethyl Ether and Ethanol, University of the Basque Country UPV/EHU, Bilbao, Spain, 2012 (Ph.D. Thesis).
[42] J.A. Torres, J. Llorca, A. Casanovas, M. Dominguez, J. Salvado, D. Montane, J. Power Sources 169 (2007) 158–166.
[43] P. Lan, Q. Xu, M. Zhou, L. Lan, S. Zhang, S. Yan, Chem. Eng. Technol. 33 (2010) 2021–2028.
[44] C.M. Kinoshita, S.Q. Turn, Int. J. Hydrogen Energy 28 (2003) 1065–1071.
[45] A.R. Fernández-Akarregi, J. Makibar, G. López, M. Amutio, M. Olazar, Fuel Process. Technol. 112 (2013) 48–56.
[46] M. Amutio, G. Lopez, M. Artetxe, G. Elordi, M. Olazar, J. Bilbao, Resour. Conserv. Recycling 59 (2012) 23–31.
[47] M. Amutio, G. Lopez, R. Aguado, M. Artetxe, J. Bilbao, M. Olazar, Fuel 95 (2012) 305–311.
[48] A.G. Gayubo, B. Valle, A.T. Aguayo, M. Olazar, J. Bilbao, J. Chem. Technol. Biotechnol. 85 (2010) 132–144.
[49] X. Wang, Y. Wei, J. Zhang, H. Xu, W. Li, React. Kinet. Catal. Lett. 89 (2006) 97–104.
[50] B. Vos, E. Poels, A. Bliek, J. Catal. 198 (2001) 77–88.
[51] B.M. Vogelaar, A.D. van Langeveld, P.J. Kooyman, C.M. Lok, R.L.C. Bonné, J.A. Moulijn, Catal. Today 163 (2011) 20–26.
[52] B.W. Hoffer, A.D. van Langeveld, J. Janssens, R.L.C. Bonné, C.M. Lok, J.A. Moulijn, J. Catal. 192 (2000) 432–440.
[53] O. Clause, B. Rebours, E. Merlen, F. Trifiró, A. Vaccari, J. Catal. 133 (1992) 231–246.
[54] J. Richardson, B. Turk, M. Twigg, Appl. Catal. A 148 (1996) 97–112.
[55] H. Jin, T. Okamoto, M. Ishida, Ind. Eng. Chem. Res. 38 (1999) 126–132.
[56] X. Chen, Y. Liu, G. Niu, Z. Yang, M. Bian, A. He, Appl. Catal. A 205 (2001) 159–172.
[57] A. Barrera, S. Fuentes, M. Viniegra, A. Avalos-Borja, N. Bogdanchikova, J. Campa-Molina, Mater. Res. Bull. 42 (2007) 640–648.
[58] A. Remiro, B. Valle, A.T. Aguayo, J. Bilbao, A.G. Gayubo, Fuel Process. Technol. 115 (2013) 222–232.
[59] H.S. Bengaard, J.K. Nørskov, J. Sehested, B.S. Clausen, L.P. Nielsen, A.M. Molenbroek, J.R. Rostrup-Nielsen, J. Catal. 209 (2002) 365–384.
[60] C. Bartholomew, Appl. Catal. A 212 (2001) 17–60.
[61] X.E. Verykios, Int. J. Hydrogen Energy 28 (2003) 1045–1063.